Two-dimensional natural element analysis of double-free surface flow under a radial gate

Farhang Daneshmand, S.A. Samad Javanmard, Jan F. Adamowski, Tahereh Liaghat, and Mohammad Mohsen Moshksar

Abstract: The gravity-driven free surface flow problems for which both the solid and free surface boundaries are highly curved are very difficult to solve. A computational scheme using a variable domain and a fixed domain natural element method (NEM) is developed in the present study for the computation of the free surface profile, velocity and pressure distributions, and the flow rate of a 2D gravity fluid flow through a conduit and under a radial gate. The problem involves two highly curved unknown free surfaces and arbitrary curved-shaped boundaries. These features make the problem more complicated than flow under a sluice gate or over a weir. The fluid is assumed to be inviscid and incompressible and the results obtained are confirmed by conducting a hydraulic model test. The results are in agreement with other flow solutions for free surface profiles and pressure distributions.

Key words: free surface flow, natural neighbour interpolation, numerical methods, hydraulic gates.

Résumé : Les problèmes d'écoulement gravitaire en surface libre où les limites imposées par les parois solides et la surface libre sont très courbes sont très difficiles à résoudre. Un modèle informatique utilisant une méthode d'éléments naturels à domaine variable et à domaine fixe est développée dans la présente étude afin de calculer le profil de la surface libre, les distributions de vitesse et de pression ainsi que le débit d'un écoulement gravitaire bidimensionnel d'un fluide dans un conduit et sous une vanne à segment. Le problème implique deux surfaces libres inconnues très courbées et des limites courbes arbitraires. Ces caractéristiques rendent le problème plus compliqué que celui de l'écoulement sous une vanne registre ou par-dessus un déversoir. Il est présumé que le fluide est incompressible et non visqueux; les résultats obtenus sont confirmés par un essai utilisant un modèle hydraulique. Les résultats concordent avec les autres solutions d'écoulement pour les profiles à surface libre et les distributions de pression.

Mots-clés : écoulement en surface libre, interpolation du voisin naturel, méthodes numériques, écluses hydrauliques.

[Traduit par la Rédaction]

Introduction

Various types of hydraulic structures are commonly used in rivers and channels as control structures. Examples of these control structures include spillways, weirs, and various types of gates. The fluid loads on such structures and the free surface profiles of the flow have to be determined for design purposes. This is a difficult task because the determination of the free surface location as a part of the solution involves the solution of an intrinsically nonlinear problem. Neither the location of the free surface nor the magnitude of the flow discharge is known a priori and to date, no exact solutions have been proposed. Using analytical methods such as conformal mapping for solving the problem are limited in number due to the necessity to establish certain mapping relations and the difficulty in satisfying the nonlinear boundary condition of constant pressure along the free surface. Moreover, the nonlinear nature of the problem dictates a numerical solution procedure at the end of such analysis (Larock 1970; Petrila 2002).

Among the many numerical methods, the finite element method (FEM) (Ikegawa and Washizu 1973; Chan et al. 1973; Bettess and Bettess 1983; Abdel-Malek et al. 1989; Sankaranarayanan and Rao 1996; Daneshmand et al. 2000) and the boundary-element method (Cheng et al. 1981) have gained popularity. Most of these methods have been successfully applied to the cases of flows over spillways or under sluice gates with only one free surface and a simple geometry. Regarding the difficulty associated with remeshing in FEM, the past decade has seen a tremendous surge in the development of a family of Galerkin and collocation based numerical methods known as meshless methods (Belytschko et al. 1994; Liu et al. 1995; Daneshmand and Niroomandi 2007). The natural element method (NEM) is a Galerkin

F. Daneshmand and J.F. Adamowski. Department of Bioresource Engineering, Faculty of Agricultural and Environmental Sciences, McGill University, 21111 Lakeshore Road, Ste. Anne de Bellevue, QC H9X 3V9, Canada.
S.A.S. Javanmard and M.M. Moshksar. Mechanical Engineering Department, Marvdasht Branch, Islamic Azad University, Marvdasht, Iran.
T. Liaghat. Mechanical Engineering Department, École Polytechnique de Montréal, P.O. Box 6000, Montréal, QC H3C 3A7, Canada.

Corresponding author: Farhang Daneshmand (e-mail: farhang.daneshmand@mcgill.ca).

Fig. 1. Fluid flow through a conduit and under the radial gate.
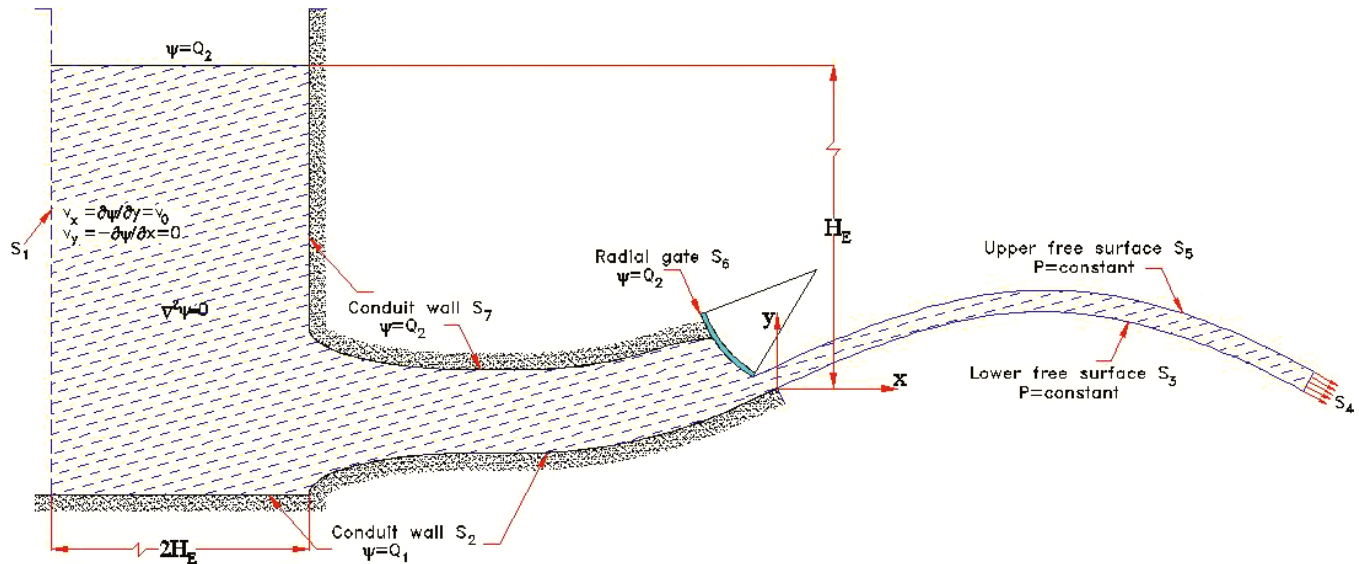
based method that is built upon Voronoi diagrams and Delaunay tessellations (Sukumar et al. 2001). This interpolation scheme has several very useful properties, such as its strictly interpolating character, its ability to exactly interpolate piecewise linear boundary conditions, and a well-defined and robust approximation with no user-defined parameter on nonuniform grids. Yvonnet et al. (2004) provided a detailed review on natural neighbour interpolation and its drawbacks in non-convex domains. González et al. (2007) presented a natural neighbour Galerkin method in conjunction with α-shapes for the numerical simulation of free-surface dynamics of flows within an updated Lagrangian treatment. Recently, Daneshmand et al. (2010) presented a numerical procedure based on natural element discretization that treats the fluid flow through a sluice gate with a free surface.

Despite some progress in solving gravity driven free surface flows with various numerical methods, solving the problem with two highly curved free surfaces via the use of NEM has not been investigated. Fluid flows that are driven by gravity and in which the solid and free surface boundaries are highly curved are considerably more complicated. Such situations occur, for instance, in the case of flow under a radial gate placed at the end of a conduit. In this case, a large extent of the free water jet downstream of the gate has to be considered in determining the pressure distribution along the gate. In addition to these characteristics, the free jet flow has two unknown free surfaces to be determined and is therefore more difficult to manage. Our aim is to present a numerical procedure based on natural element discretization that treats the fluid flow through a gate with two highly curved free surfaces and arbitrary shaped boundaries. The novel features of the present study are that (1) it involves two free surfaces and (2) the free surfaces are relatively long and have a more curved shape than the flow under a sluice gate or over a spillway. In the present study, lower and upper free surface profiles, velocity and pressure distributions, and flow rate per unit width Q are calculated for a known Bernoulli constant, B, using the natural element method. Results for pressure distribution are compared with measured values obtained by conducting a hydraulic model test.

Problem formulation and discretization

Flows under radial gates can be considered as rapidly converging flows in which the influence of fluid viscosity is quite small in comparison with interial effects, and consequently, in almost all studies of problems of this type, we can assume that the flow is irrotational. A typical two-dimensional steady flow from a reservoir, through an arbitrary shaped conduit and under a radial gate in the pattern of a free jet is shown in Fig. 1. Geometry of the conduit walls S_2 and S_7 are given and the far upstream and downstream boundaries of the flow domain, denoted by S_1 and S_4 are assumed to be normal and perpendicular to the flow direction, respectively. The boundary S_6 is the surface of the radial gate and can be considered as a fixed solid boundary. The lower and upper free surface profiles S_3 and S_5 are not known a priori. Either, the flow discharge per unit width of conduit is given and the stagnation level and flow field are sought, or the stagnation level is given and the corresponding rate of flow per unit width of channel is to be determined. In the present study, the flow rate Q is assumed to be unknown and the stagnation level is given as H_E, which is the stagnant fluid level above point A. For convenience, the origin of the coordinate system is located as shown in Fig. 1. The horizontal and vertical coordinates are denoted by x and y, respectively.

For the two-dimensional potential flow, the flow velocities v_x and v_y is defined in terms of a stream function (ψ)

[1] $v_x = \psi_{,y} \quad v_y = -\psi_{,x}$

and the flow is governed by the Laplace equation,

[2] $\psi_{,xx} + \psi_{,yy} = 0 \quad \text{on } \Omega$

where ψ is the stream function, Ω is the flow domain bounded by the aforementioned boundaries, and comma denotes differentiation. The numerical solution of partial differential eq. [2] requires some form of spatial discretization. Basically, there are two different types of specification for the flow field, Lagrangian and Eulerian. We can think of the Lagrangian mesh as being drawn on the body. The mesh de-

Fig. 2. Definition of the natural neighbour coordinates in NEM: (*a*) original Voronoi diagram and (*b*) first-order and second-order Voronoi cells about *x* (modified from Cueto et al. 2003).
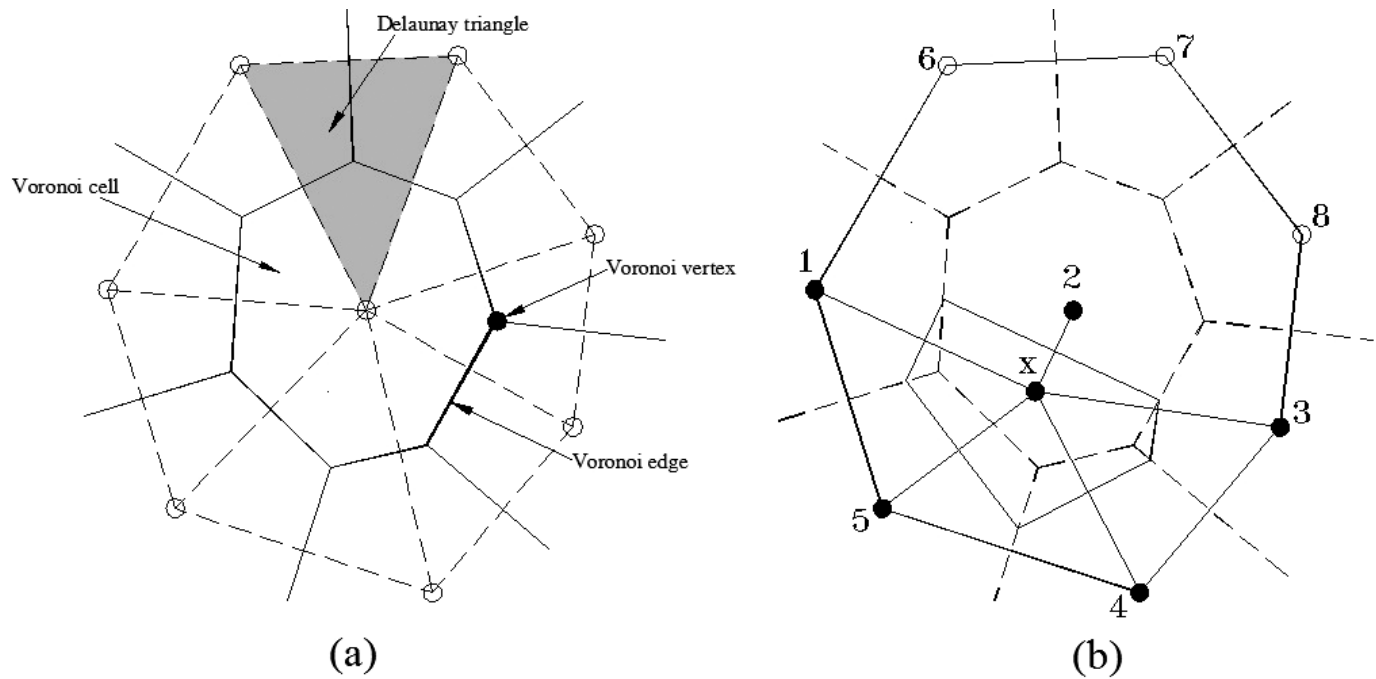
forms with the body and both the nodes and the material points change position as the body deforms. However, the position of the material points relative to the nodes remains fixed. On the other hand, the Eulerian mesh is a background mesh. The body flows through the mesh as it deforms. The nodes remain fixed and the material points move through the mesh. The position of a material point relative to the nodes varies with the motion. The natural element method which is based on the Lagrangian approach is used in the present study. As the first step in the numerical solution, the problem domain is divided into elements with a suitable interpolation model assumed for $\psi^{(e)}$ as

[3] $\qquad \psi^{(e)}(x, y) = \sum_{i=1}^{m} \varphi_i(x, y)\psi_i^{(e)}$

where $\varphi_i(x, y)$ is the natural element interpolation function as given in the next section and *m* is the number of neighborhoods of point (*x*, *y*).

The boundary conditions of the problem are

[4] $\qquad \psi = 0$ on S_2 and S_3

[5] $\qquad \psi = Q$ on S_5, S_6 and S_7

[6] $\qquad \psi_{,n} = -\sqrt{2gz}$ on S_3 and S_5

[7] $\qquad \psi_{,n} = 0$ on S_1 and S_4

It should be noted that for the purposes of the numerical solution, outflow streams are cut at right angles to the primary velocity. Boundary condition eq. [7] is applied on this part, which means that there is no velocity normal to the main flow. Here, *n* is the outward normal to the boundary, *z* is the distance of the free surface from the datum line of the

stagnation level, and *g* is the gravitational acceleration. The problem is to find the corresponding upper and lower free surface profile, together with the velocity field, in particular the pressure distribution on the gate by solving eq. [2] subject to the boundary conditions eqs. [4]–[7], given either the total head H_E or the flow rate *Q*. In the present study, H_E is given and *Q* is found as part of the solution.

Voronoi diagrams and Delaunay tessellations

Classical definitions for Voronoi diagrams and Delaunay tessellations as used in NEM can be found in Yvonnet et al. (2004) and González et al. (2007). The first-order Voronoi diagram of the set $N = \{n_1, n_2, \ldots, n_M\}$ is a sub-division of the space into regions T_I, such that any point in T_I is closer to n_I than to any other node of the set. The region T_I is the Voronoi cell of n_I and is defined as

[8] $\qquad T_I = \{x \in R^2 : d(x, x_I) < d(x, x_J) \, \forall J \neq I\}$

where $d(x_I, x_J)$ is the Euclidean distance between x_I and x_J. The Delaunay tessellation is constructed by connecting nodes whose Voronoi cells have common boundaries (Fig. 2*a*). An important property of Delaunay triangles is that the circumcircle of any Delaunay triangle of the nodal set *N* contains no other nodes of *N*. Introduction of a point *X* into the problem domain Ω, the Voronoi cells for the point *X* and its natural neighbours are shown in Fig. 2*b* (Cueto et al. 2003). In this section, Sibson and non-Sibsonian (Laplace) interpolation schemes (Sukumar et al. 1998; Sukumar and Moran 1999; Cueto et al. 2003) are reviewed, although only Sibson interpolation will be used in the examples included in this paper.

For the Sibson shape functions the natural neighbour coordinates of *x* are defined as the ratio of the area of overlap of their Voronoi cells to the total area of the Voronoi cell of *x* (Fig. 2*a*),

Fig. 3. Construction of non-Sibsonian interpolants (modified from Sukumar et al. 2001).
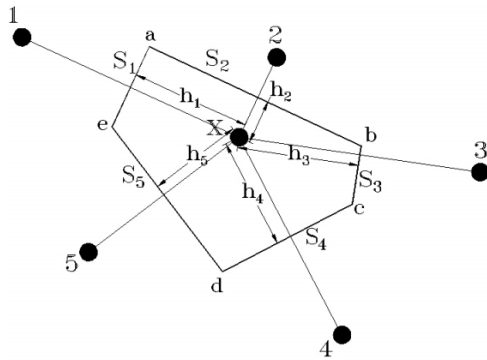
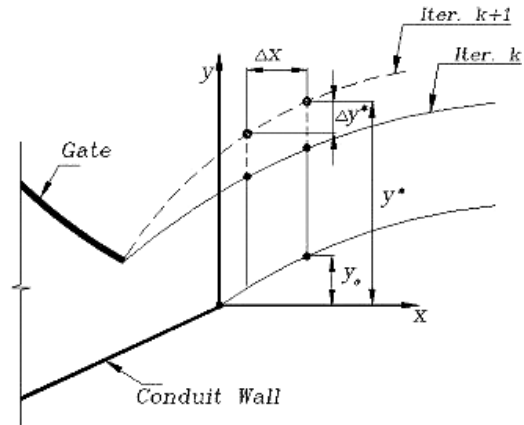$$[9] \qquad \Phi_I(x) = \frac{A_I(x)}{A(x)}$$

The first derivatives of the shape functions are

$$[10] \qquad \Phi_{I,j}(x) = \frac{A_{I,j}(x) - \Phi_I(x)A_{,j}(x)}{A(x)} \quad (j = 1, 2)$$

In two dimensions, the non-Sibsonian shape function $\Phi_I(x)$ takes the form

$$[11] \qquad \Phi_I(x) = \frac{\alpha_I(x)}{\displaystyle\sum_{J=1}^{n} \alpha_J(x)} \quad \alpha_J(x) = \frac{s_J(x)}{h_J(x)}$$

Fig. 4. Node adjustment.

where $s_I(x)$ is the length of the Voronoi edge associated with node I and $h_I(x)$ is the perpendicular distance between the Voronoi edge of node I to x (Fig. 3). The derivative of the non-Sibsonian shape function is obtained by differentiating eq. [11] as

$$[12] \qquad \Phi_{I,j}(x) = \frac{\alpha_{I,j}(x) - \Phi_I(x)\alpha_{,j}(x)}{\displaystyle\sum_{J}\alpha_J(x)} \quad (j = 1, 2)$$

Multiplying the governing eq. [2] by φ_i selected according to the Galerkin approach, we get

$$[13] \qquad \iint\limits_{\Omega^{(e)}} \varphi_i\left(\psi_{,xx}^{(e)} + \psi_{,yy}^{(e)}\right) \mathrm{d}\Omega = \iint\limits_{\Omega^{(e)}} \varphi_i\left(\varphi_{i,x}\psi_{,x}^{(e)} + \varphi_{i,y}\psi_{,y}^{(e)}\right)\mathrm{d}\Omega - \int\limits_{\Gamma^{(e)}} \varphi_i\left(\psi_{,x}^{(e)}n_x + \psi_{,y}^{(e)}n_y\right)\mathrm{d}\Gamma = 0$$

where $\Omega^{(e)}$ and $\Gamma^{(e)}$ denote the domain and boundary of element (e), respectively. Using the integration by-parts and boundary conditions given in eqs. [4] to [7] and the procedure given in Daneshmand et al. (2010), the discretized form of eq. [13] leads to the following system of equations in matrix form:

$$[14] \qquad \mathbf{K}\boldsymbol{\psi} = \boldsymbol{P}$$

where $\mathbf{K}$ is the total system matrix for the problem, $\boldsymbol{\psi}$ is the vector including the unknown nodal values of the stream function, and $\boldsymbol{P}$ is the total load vector. It should be noted that the system matrices $\mathbf{K}$ and $\mathbf{P}$ are obtained by assembling the following element matrices:

$$[15] \qquad \mathbf{K}^{(e)} = \iint\limits_A \mathbf{B}^T\mathbf{B}\mathrm{d}A \quad \mathbf{B} = \begin{bmatrix} \varphi_{1,x} & \varphi_{2,x} & \cdots & \varphi_{m,x} \\ \varphi_{1,y} & \varphi_{2,y} & \cdots & \varphi_{m,y} \end{bmatrix}$$

$$[16] \qquad \mathbf{P}^{(e)} = -\int\limits_\Gamma V_0\mathbf{N}^T\mathrm{d}\Gamma \quad \mathbf{N}^T = \begin{bmatrix} \varphi_1 & \varphi_2 & \cdots & \varphi_m \end{bmatrix}$$

where A and Γ are the area and boundary of an element, respectively.
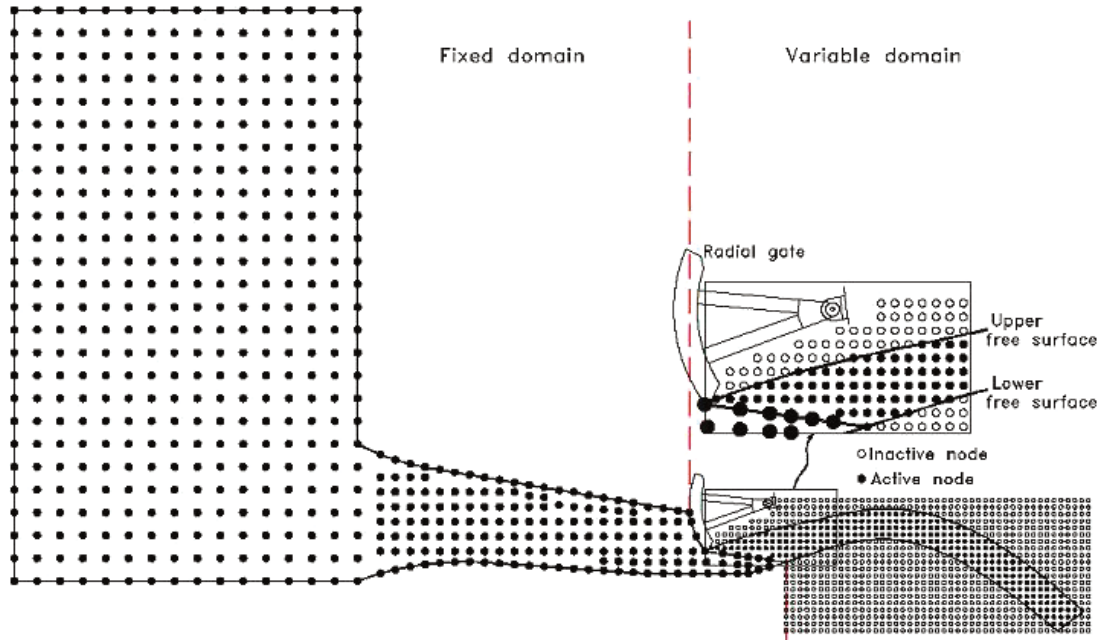
Iteration for the free surfaces

The constant pressure condition on the upper and lower free surfaces requires

$$[17] \qquad \frac{1}{2g}\left(\frac{\partial\psi}{\partial n}\right)^2 + y = B$$

where y is the free surface elevation, g is the gravity acceleration, and B is the Bernoulli constant. When the Bernoulli constant, B, is known, the problem is first solved by assuming the location of the free surfaces and applying the boundary conditions, eqs. [4]–[7]. The solution yields different values of the stream function at each of the free surface nodes. If the stream function is constant for all points on the free surfaces, the problem is solved; otherwise, an iteration scheme must be used to adjust the free surface elevation. The calculated value of the stream function ψ^k at the start point of the free surface is considered as a good estimation for Q^{k+1} to perform the free surface adjustment in the next iteration. The x and y-components of the velocity for free surface nodes are calculated by using equation eq. [1]. By satisfying the zero normal velocity condition on the free surfaces, the free surface correction can be achieved by using the following relations (Fig. 4) (Daneshmand et al. 2000):

Fig. 5. Active and inactive nodes in fixed and variable domain.

$$[18] \quad \begin{cases} \Delta y^* = \dfrac{\beta \Delta x}{6}(\alpha_1 + \alpha_2 + \alpha_3) & \text{when } \Delta y > 0 \\[2mm] \Delta y^* = \dfrac{\Delta x}{6\beta}(\alpha_1 + \alpha_2 + \alpha_3) & \text{when } \Delta y < 0 \end{cases}$$

where β is the correction factor for the free surface and α_1, α_2, and α_3 are the slopes of the velocities at three successive nodes on the free surface and can easily be obtained by using their x and y-velocity components.

Although it is theoretically possible to assume the location of both the lower and the upper free surfaces, test calculations of this kind have proven to be time consuming with convergence problems. Instead, an alternating iterative procedure is used in this study. The lower and upper free surfaces are approximated in the first iteration. Then the lower free surface location is kept fixed while the upper free surface is allowed to vary. The same procedure is repeated until both the lower and the upper free surfaces converge with a specified accuracy. According to this procedure, the computer implementation of the present numerical procedure includes the following steps:

Step 1. As shown in Fig. 5, the initial problem domain is divided into fixed and variable domains. In the fixed domain, all nodes are active whereas node activation depends on the node positions in the variable domain.

Step 2. The initial trial upper and lower free surface profiles are assumed.

Step 3. The lower free surface profile is assumed to be fixed. Dirichlet and Neumann boundary conditions are applied to the nodes on the lower and upper free surface profiles, respectively. Moreover, the number of neighborhoods for any point of a triangular element in FEM is three whereas the number of neighborhoods in NEM can be greater than three. For three typical points of a triangular element as $a(x_1, y_1)$, $b(x_2, y_2)$, and $c(x_3, y_3)$, matrix **B** is evaluated by using eq. [15] as

Table 1. Karun-III dam specifications (example 1).

Type of dam	Arch concrete dam
Height (from the river bed)	205 m
Length	462 m
Base width	29.5 m
Spillway capacity	15 000 m³/s
Reservoir capacity	2 970 000 000 m³
Surface area	48 km²

$$[19] \quad \mathbf{B} = \frac{1}{2A^{(e)}} \begin{bmatrix} y_2 - y_3 & y_3 - y_1 & y_1 - y_2 \\ x_3 - x_2 & x_1 - x_3 & x_2 - x_1 \end{bmatrix}$$

where $A^{(e)}$ is the element area. It is necessary to use a suitable algorithm for finding the shape functions and their derivatives for evaluating matrix **B**.

Step 4. The problem is solved using the proposed method and the values of the stream function (ψ) for all nodes are calculated as a function of the assumed upper free surface profile. The flow rate Q^{k+1}_{upper} can then be calculated and the upper free surface is corrected by eq. [18]. The iteration process is continued until the maximum value of the convergence criterion defined as $|Q^{k+1} - \psi^k_i|/Q^{k+1}$ is less than a prescribed accuracy ε (for upper free surface).

Step 5. The upper free surface profile is assumed to be fixed and Dirichlet and Neumann boundary conditions are applied to the nodes on the upper and lower free surfaces, respectively.

Step 6. The problem is solved and the value of discharge (ψ) is calculated for all nodes as a function of the assumed lower free surface profile. The flow rate Q^{k+1}_{lower} can be calculated and the lower surface is corrected according to eq. [18]. The iteration process is continued until the maximum value of the convergence criterion defined as $|Q^{k+1} - \psi^k_i|/Q^{k+1}$ is less than a prescribed accuracy ε (for lower free surface).

Step 7. The above steps (3 to 6) are repeated until a pre-

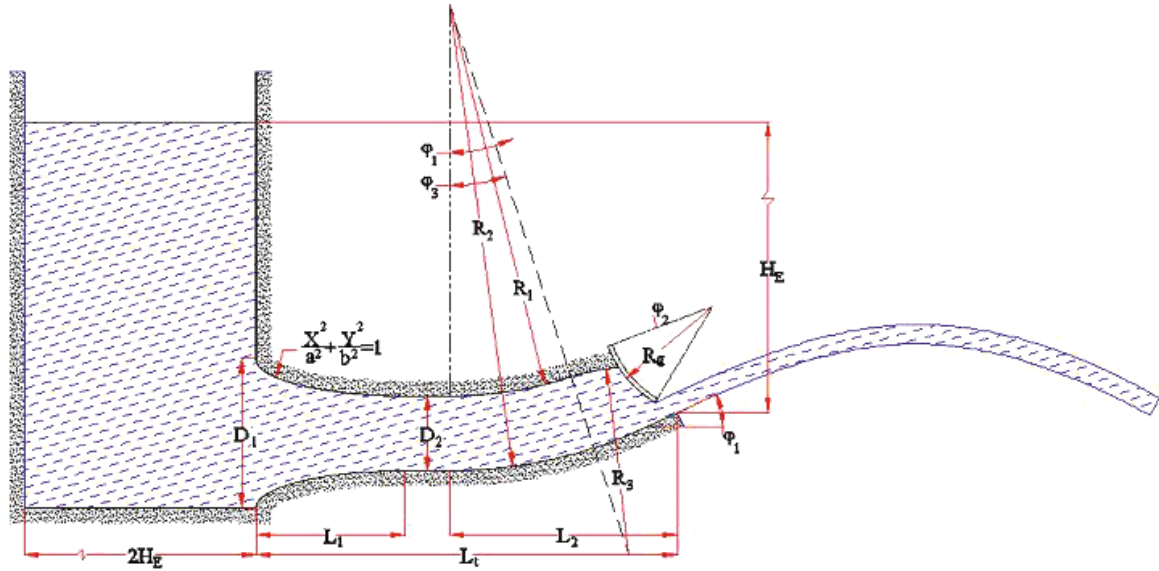**Fig. 6.** Geometry of the orifice radial gate of Karun-III.

Table 2. Technical specifications of Karun-III (example 1).

$R_1 = 1.680$ m	$R_2 = 2.000$ m	$R_3 = 0.800$ m	$R_g = 0.480$ m
$L_1 = 0.640$ m	$L_2 = 0.977$ m	$L_t = 1.8084$ m	$H_E = 3.480$ m
$\varphi_1 = 25°$	$\varphi_2 = 38.5°$	$\varphi_3 = 18.066°$	$a = 16$
$D_1 = 0.640$ m	$D_2 = 0.320$ m	$b = 4$	

scribed error criterion is satisfied on the differences in coordinates of all free surface nodes between successive iterations; that is

[20] $\qquad |y_i^r - y_i^{r-1}| \le \delta \quad \text{for} \quad i = 1, \ldots, N_s$

where y_i^r and y_i^{r-1} are y-coordinates of node i on the free surface at iterations r and $r–1$, respectively; N_s is the number of free surface nodes; and δ is the prescribed accuracy for nodes positions.

Results

The numerical procedure described above was applied to flow under radial gates in two different cases. For both examples, the results of the present study were compared with those obtained from a hydraulic model test.

Example 1 — Karun-III dam

The Karun-III dam is a hydroelectric dam on the Karun River in the province of Khuzestan, Iran. It was built to help meet energy demands as well as to provide flood control. The Karun has the highest discharge of Iran's rivers. The dam is a concrete double arch type dam, 205 m above the foundation and 185 m above the river bed. Its foundation width is 29.5 m (Table 1). The geometry and specifications of the orifice radial gate of Karun-III dam are also given in Fig. 6 and Table 2. To ensure the validity of the results obtained for this example, a hydraulic model test based on the Froude law of similarity was also constructed (Sadid-Tadbir Company 1997). The hydraulic pressures were measured by pressure transducers with a rate of 200 samples per second. A simple weir, located at the conduit downstream from the liner, was used to measure the amount of water discharged.

A combination of a fixed and variable domain natural element method as proposed in this study was used in this example. The matrix corresponding to the elements in the fixed domain was calculated only once whereas the stiffness matrix related to the elements in the variable region (free surface region) should be calculated in successive iterations while an adjustment of the free surface is made. The prescribed accuracy is defined by ε. To solve the problem by the natural element method, 591 nodes and 952 elements are used in the first iteration. In this example, the convergence was obtained after three iterations with 6–15 nested iterations on each free surface for $\varepsilon = 0.005$. The computed discharge is $Q = 0.502$ m$^3 \cdot$s$^{-1} \cdot$m^{-1}, which is in agreement with the value obtained from the experiment $Q = 0.485$ m$^3 \cdot$s$^{-1} \cdot$m^{-1}. The pressure distribution in the liner, obtained from the natural element procedure is shown in Fig. 7 and is compared with those obtained from the hydraulic model test. Figure 8 gives the pressure distribution on the radial gate obtained from the numerical and experimental analysis. The shapes of upper and lower free surfaces are also plotted in Fig. 9.

Example 2 — Shahryar Dam

The construction of the Shahryar Dam and the powerhouse plant will be carried out with a 700 million m^3 capacity reservoir and the ability to regulate 1100 million m^3 of water by itself and 3218 million m^3 of water along with the Sefidrood Dam (located 34 km from the town of Mianeh and across the Qhzlozan River in the eastern Azerbaijan province of Iran). The Shahryar Dam is a double curvature concrete arch dam with a height of 135 m. The dam specifications are given in Table 3.

The bottom outlet of the dam is equipped with a maintenance intake gate, an emergency gate, and a radial service

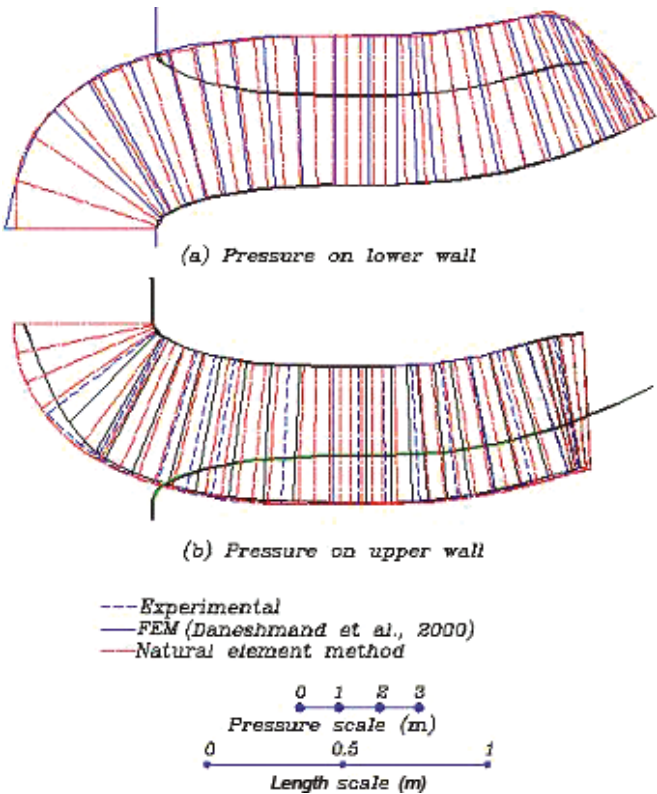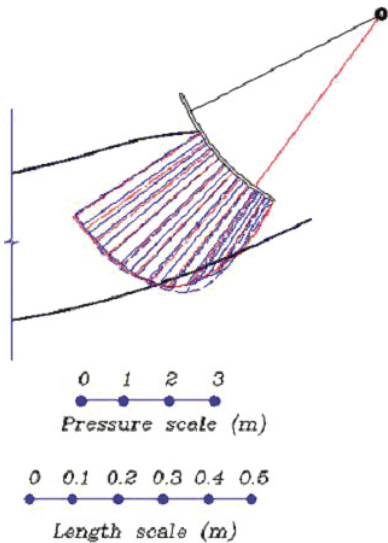**Fig. 7.** Pressure distribution on conduit walls (example 1).

(a) Pressure on lower wall

(b) Pressure on upper wall

---Experimental
—FEM (Daneshmand et al., 2000)
—Natural element method

0 1 2 3
Pressure scale (m)

0   0.5   1
Length scale (m)

Fig. 8. Pressure distribution on the radial gate (example 1).

0 1 2 3
Pressure scale (m)

0 0.1 0.2 0.3 0.4 0.5
Length scale (m)

Table 3. Shahryar Dam specifications (example 2).

Parameter	Value (description)
Type	Double-arch concrete dam
Height (from the river bed)	135 m
Crest elevation	1045 m.a.s.l.
Bottom outlet sill elevation	1004 m.a.s.l.
Total storage (at normal water level)	700 MCM
Normal water level	1035 m.a.s.l.
Maximum water level	1041 m.a.s.l.

Note: m.a.s.l. is metres above sea level.

Table 4. Specifications of the bottom outlet gates (example 2).

Radial gate	
Type	Radial gate
Discharge at normal water level	250 m^3/s
Radius	5.2 m
Width	3.8 m
Opening	3×4 m (w $\times$ h)
Maneuvering speed	0.3 m/min
Sealing type	Rubber seal
Maintenance gate	
Type	Fixed wheel gate
Dimensions	3.85×6.2 m (w $\times$ h)
Corrosion	2 mm
Bed elevation	1005.75 m
Emergency gate	
Type	Roller gate
Discharge at normal water level	250 m^3/s
Dimensions (gate/opening)	3.0×4.2 m (w $\times$ h)
Maneuvering speed	0.3 m/min
Sealing type	double stem rubber seal

Table 5. Technical specification for radial gate (example 2).

Parameter	Value	Parameter	Value
a	1.15	i	0.167
b	0.08	h	2.5
c	0.44	R_1	1
d	0.71	R_2	1.33
e	0.55	R_g	0.347
f	1.5	θ	10°
g	2.4	β	163°

Table 6. Dependence of the algorithm to the initialization step (example 2).

Lower free surface profile (Fig. 13)	Number of iterations
1	105
2	93
3	81
4	70
5	53
6	46

gate (Table 4). The maintenance gate is used for maintenance work of downstream equipment and is operated under the balanced pressure condition attained by means of a by-pass valve in the gate leaf. The service gate of the outlet is a radial gate. The definition sketch and technical specifications of the radial service gate are given in Fig. 10 and Table 5, respectively.

The value of head loss was calculated using the procedure given in Roberson and Clayton (1997) for the entrance loss (loss coefficient = 0.03) and Brno Technical University (1994) for the outlet loss due to sudden contraction, respectively. To ensure the validity of the results obtained in this ex-

ample, a hydraulic model test (scale 1:15) based on Froude's law of similarity was also constructed (Shiraz University 2007). The hydraulic model test included the entire passage of water both upstream and downstream of the gate. The hy-

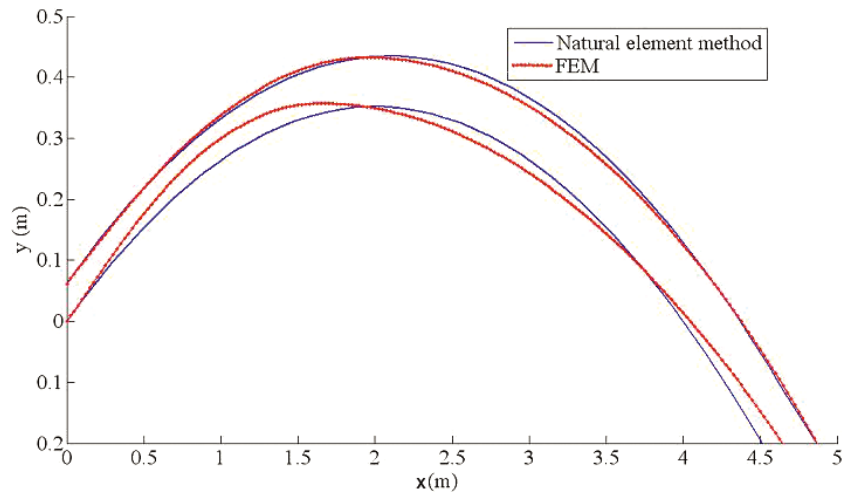**Fig. 9.** The shapes of the upper and lower free surfaces (example 2).

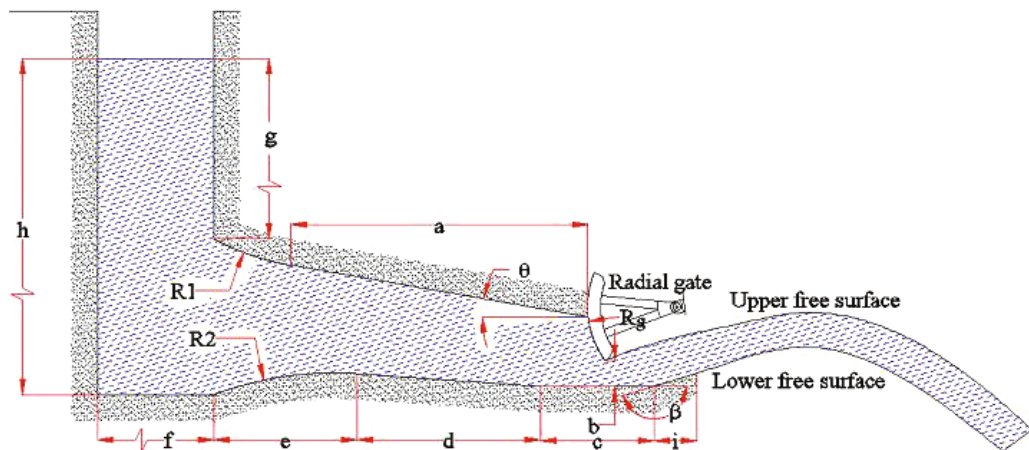**Fig. 10.** Bottom-outlet radial service gate of Shahryar Dam (example 2).

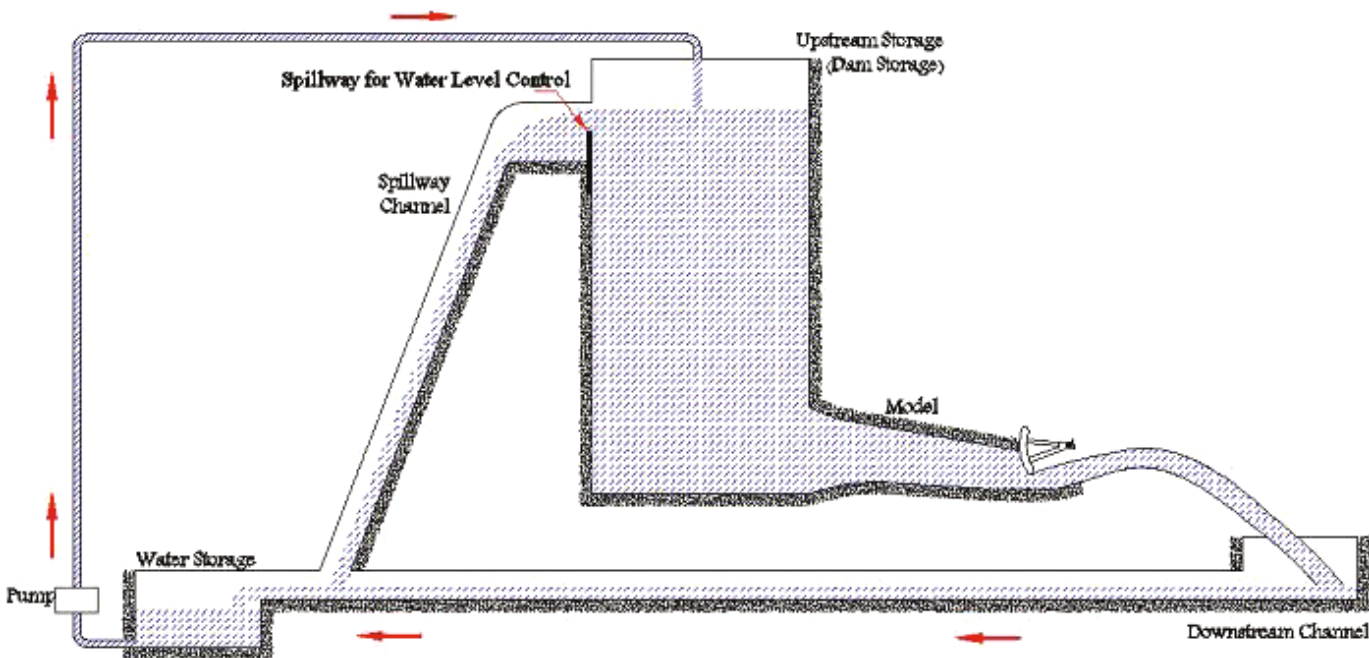**Fig. 11.** Test stand for hydraulic model test (example 2).

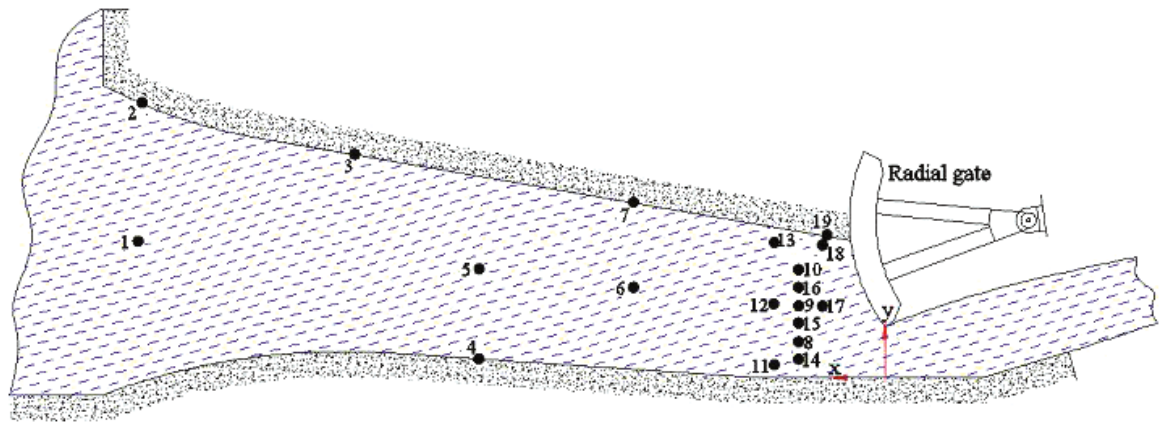**Fig. 12.** Locations of pressure measuring points (example 2).

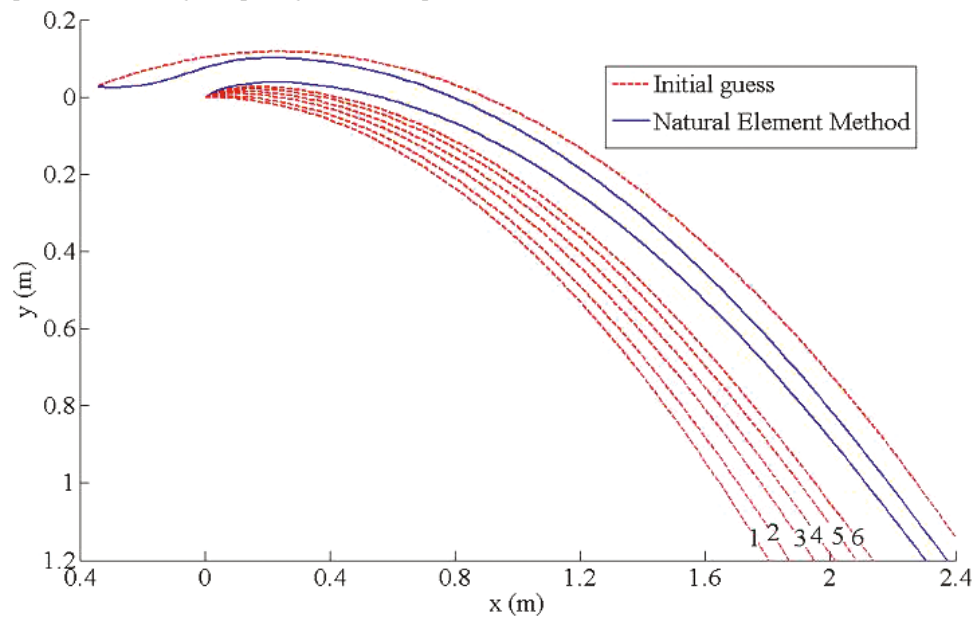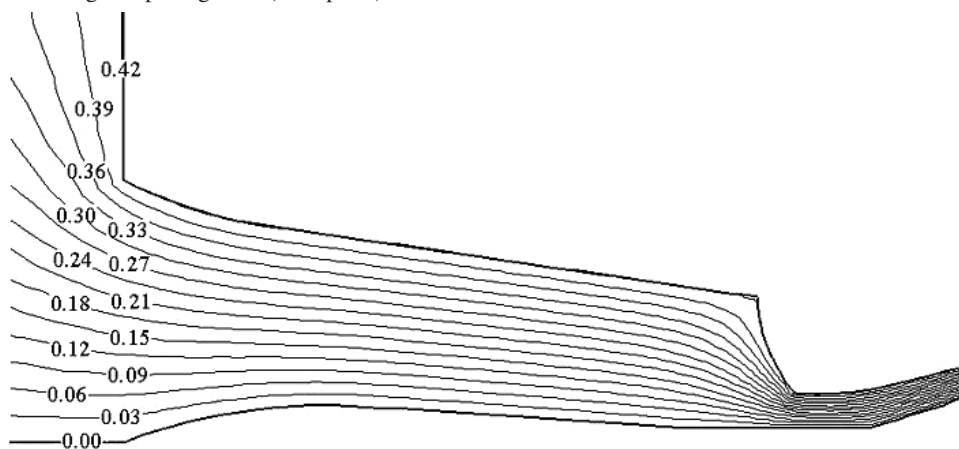**Fig. 13.** Free surface profile for radial gate opening 30% (example 2).

Table 7. Comparison between numerical and experimental results (example 2).

Mano. No.	x (m)	y (m)	p (mH$_2$O) model test	p (mH$_2$O) NEM	Error (%)	ψ (m^3/s) NEM	v (m/s) NEM
1	1.4481	0.2643	2.2033	2.1658	1.7	0.2123	0.8461
2	1.4400	0.5250	1.9060	1.8835	1.2	0.4492	1.0678
3	1.0280	0.4332	2.0033	1.9665	1.9	0.4473	1.1462
4	0.7870	0.0364	2.3660	2.3506	0.7	0.0017	1.2500
5	0.7875	0.2107	2.2080	2.1778	1.4	0.2179	1.2388
6	0.4875	0.1752	2.2147	2.2016	0.6	0.2144	1.3282
7	0.4875	0.3401	2.0593	2.0404	0.9	0.4286	1.3008
8	0.1675	0.0697	2.2513	2.1930	2.7	0.1447	1.9986
9	0.1675	0.1397	2.1620	2.1805	0.8	0.2648	1.6905
10	0.1675	0.2093	2.1373	2.1725	1.6	0.3548	1.2840
11	0.2146	0.0250	2.3420	2.2757	2.9	0.0447	1.8039
12	0.2159	0.1430	2.2293	2.2053	1.1	0.2397	1.5224
13	0.2146	0.2620	2.1013	2.1355	1.6	0.3899	1.1633
14	0.1675	0.0360	2.2973	2.2051	4.2	0.0762	2.0995
15	0.1675	0.1058	2.1880	2.1862	0.1	0.2094	1.8464
16	0.1675	0.1750	2.1473	2.1805	1.5	0.3130	1.4687
17	0.1211	0.1390	2.2173	2.1369	3.8	0.3046	1.9220
18	0.1211	0.2570	2.1893	2.1769	0.6	0.4236	0.7998
19	0.1125	0.2768	2.1740	2.1711	0.1	0.4385	0.5938

Fig. 14. ψ contour for radial gate opening 30% (example 2).

Fig. 15. Velocity contour for radial gate opening 30% (example 2).
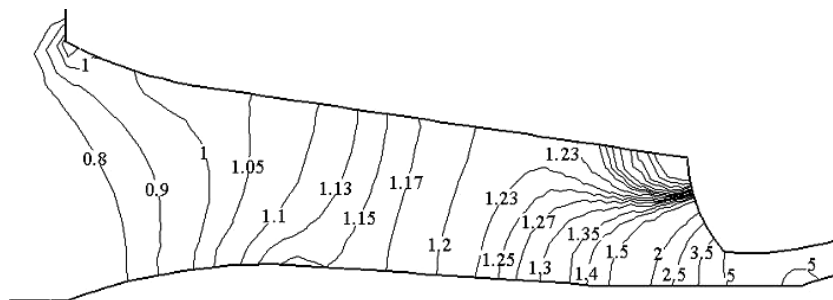
draulic model was constructed using plexiglass material to secure good flow visualization. For better visualization of the free surface profile, the downstream wall of the model was meshed by squares 5 cm × 5 cm. The test stand included three centrifugal pumps, as well as main water storage and relevant channels to complete the closed loop circuit (Fig. 11).

For measuring pressure, manometers were installed at different points in the channel and a skin plate was positioned on the gate. The locations of pressure measuring points are shown in Fig. 12. The unit of measured pressure is mH$_2$O. Water discharge was also measured by using the area–velocity flow meter (Greyline AVFM-II). Its ultrasonic sensor was installed at the bottom of the downstream channel. Based on the speed of sound in the water, the level was measured with an accuracy of ±0.25%. Flow velocity was also measured with an ultrasonic Doppler signal. The instrument measures velocity with an accuracy of ±0.2%.

The radial gate is considered to be in a 30% opening position and the natural element method with 855 nodes and 1328 elements (in the first iteration) was used to solve the problem. The discretization was made finer in the vicinity of the gate to take care of the higher velocity gradients in that region. In this example, the convergence was obtained on the free surface profiles with a prescribed accuracy $\varepsilon = 0.001$. Two values for the correction factor for lower and upper free surfaces are used in the calculations as $\beta_L = 1.20$ and $\beta_U = 1.5$, respectively. The computed discharge Q is 0.421 m^3·m^{-1}·s^{-1}, which is in good agreement with the value obtained from the experiment ($Q = 0.399$ m^3·m^{-1}·s^{-1}). The pressure values are given in Table 6 and compared with the pressure values measured in the hydraulic model test. The shape of the free surfa-

ces obtained from NEM is presented in Fig. 13. To study the dependence of the proposed algorithm to the initialization step, we re-analyzed the problem with different lower free surface trials while keeping the upper free surface fixed. As shown in Table 6 and Fig. 13, the algorithm converged for all cases with reasonable accuracy ($\varepsilon = 0.005$) and the number of iterations decreased when the initial lower free surface profile changed from 1 to 6, as expected. As can be seen from Table 6, the pressure obtained from NEM is in agreement with that obtained from the model test. It should also be noted from Table 7 that the maximum error in pressure values is 2.9%. Figures 14 and 15 show the ψ and velocity contours, respectively.

Conclusions

Hydraulic structures are used to regulate the flow of water through canals and analysis of flows with free surfaces under hydraulic gates has received a good deal of attention in the field of hydraulic engineering. Our aim in this paper was to present a numerical procedure based on the natural element method to treat the fluid flow through a radial gate with two free surfaces. We implemented the most notable aspects of the natural element method with emphasis on the recent advances achieved by the authors in its application to hydraulic structures. The natural neighbour interpolation scheme was used for construction of test and trial functions whereas the governing equations for the fluid domain of the problem were written in terms of stream function. Two practical examples were solved and the results were compared with those obtained from hydraulic model tests to validate the accuracy and convergence of the proposed method. The results were in

excellent agreement with the experiment. In spite of the non-linear nature of the present problem, a rapid rate of convergence was observed even with an initial guess that differs significantly from the actual solution. Comparing the results of the proposed numerical method with those obtained from the hydraulic model test confirms that the method is sufficiently accurate for practical purposes and can be used with confidence in calculating the hydraulic parameters needed in the design of hydraulic structures.

Acknowledgments

References

Abdel-Malek, M.N., Hanna, S.N., and Abdel-Malek, M. 1989. Approximate solution for gravity flow under a Tainter gate. Journal of Computational and Applied Mathematics, **26**(3): 271–279. doi:10.1016/0377-0427(89)90299-9.

Belytschko, T., Lu, Y.Y., and Gu, L. 1994. Element-free galerkin methods. International Journal for Numerical Methods in Engineering, **37**(2): 229–256. doi:10.1002/nme.1620370205.

Bettess, P., and Bettess, J.A. 1983. Analysis of free surface flows using isoparametric finite elements. International Journal for Numerical Methods in Engineering, **19**(11): 1675–1689. doi:10.1002/nme.1620191107.

Brno Technical University. 1994. The bottom outlet Twin Gate, Marun. Water Management Research Institute, Czech Republic.

Chan, S.T.K., Larock, B.E., and Herrmann, L.R. 1973. Free surface ideal fluid flows by finite elements. Journal of the Hydraulics Division, **99**(No. HY6): 959–974.

Cheng, A.H.-D., Liggett, J.A., and Liu, P.L.-F. 1981. Boundary calculations of sluice and spillway flows. Journal of the Hydraulics Division, **107**(No. HY10): 1163–1178.

Cueto, E., Sukumar, N., Calvo, B., Martinez, M.A., Cegonino, J., and Doblare, D. 2003. Overview and recent advances in natural neighbour galerkin methods. Archives of Computational Methods in Engineering, **10**(4): 307–384. doi:10.1007/BF02736253.

Daneshmand, F., and Niroomandi, S. 2007. Natural neighbour Galerkin computation of the vibration modes of fluid-structure systems. Engineering Computations, **24**(3): 269–287. doi:10.1108/02644400710735034.

Daneshmand, F., Sharan, S.K., and Kadivar, M.H. 2000. Finite element analysis of double-free surface flow through slit in dam. Journal of the Hydraulics Division, **126**(5): 515–522.

Daneshmand, F., Javanmard, S., Liaghat, T., Moshksar, M.M., and Adamowski, J. 2010. Numerical solution for two-dimensional flow under sluice gates using the natural element method. Canadian Journal of Civil Engineering, **37**(12): 1550–1559. doi:10.1139/L10-087.

González, D., Cueto, E., Chinesta, F., and Doblaré, M. 2007. A natural element updated Lagrangian strategy for free-surface fluid dynamics. Journal of Computational Physics, **223**(1): 127–150. doi:10.1016/j.jcp.2006.09.002.

Ikegawa, M., and Washizu, K. 1973. Finite element method applied to analysis of flow over a spillway Crest. International Journal for Numerical Methods in Engineering, **6**(2): 179–189. doi:10.1002/nme.1620060204.

Larock, B.E. 1970. A Theory for free outflow beneath radial gates. Journal of Fluid Mechanics, **41**(04): 851–864. doi:10.1017/S0022112070000964.

Liu, W.K., Jun, S., and Zhang, Y.F. 1995. Reproducing kernel particle methods. International Journal for Numerical Methods in Fluids, **20**(8–9): 1081–1106. doi:10.1002/fld.1650200824.

Petrila, T. 2002. Mathematical model for the free surface flow under a sluice gate. Applied Mathematics and Computation, **125**(1): 49–58. doi:10.1016/S0096-3003(00)00109-0.

Roberson, J.A., and Clayton, T.C. 1997. Engineering fluid mechanics. 6th ed. Wiley, New York.

Sadid-Tadbir Company. 1997. Hydraulic model test of the orifice spillway for Karun III Dam, Report No. KRM-R-002, Tehran, Iran.

Sankaranarayanan, S., and Rao, H.S. 1996. Finite element analysis of free surface flow through gates. International Journal for Numerical Methods in Fluids, **22**(5): 375–392. doi:10.1002/(SICI)1097-0363(19960315)22:5<375::AID-FLD357>3.0.CO;2-O.

Shiraz University. 2007. Hydraulic model test of bottom outlet of shahryar dam Report No. SHM-R-002. Shiraz, Iran.

Sukumar, N., and Moran, B. 1999. C Natural neighbor interpolate for partial differential equations. Numerical Methods for Partial Differential Equations, **15**(4): 417–447. doi:10.1002/(SICI)1098-2426(199907)15:4<417::AID-NUM2>3.0.CO;2-S.

Sukumar, N., Moran, B., and Belytschko, T. 1998. The natural element method in solid mechanics. International Journal for Numerical Methods in Engineering, **43**(5): 839–887. doi:10.1002/(SICI)1097-0207(19981115)43:5<839::AID-NME423>3.0.CO;2-R.

Sukumar, N., Moran, B., Semenov, A.Y., and Belikov, V.V. 2001. Natural neighbour Galerkin methods. International Journal for Numerical Methods in Engineering, **50**(1): 1–27. doi:10.1002/1097-0207(20010110)50:1<1::AID-NME14>3.0.CO;2-P.

Yvonnet, J., Ryckelynck, D., Lorong, P., and Chinesta, F. 2004. A new extension of the natural element method for non-convex and discontinuous problems: the constrained natural element method (C-NEM). International Journal for Numerical Methods in Engineering, **60**(8): 1451–1474. doi:10.1002/nme.1016.

List of symbols

A	area
b	opening value (m)
B	Bernoulli constant
$\mathbf{B}$	derivative of interpolation matrix
C_1	Dirichlet boundary condition
C_2	Neumann boundary condition
$C^{(e)}$	element boundary
d_1, d_2	conduit height at inbound and outbound section (m)
g	acceleration due to gravity ($g = 9.806$ m/s^2)
$K^{(e)}$	element system matrix
$\mathbf{K}$	total system matrix
m	number of neighborhoods of any point
n	unit normal from the free surface
p	Pressure (mH$_2$O)
$\mathbf{P}$	total load vector
$P^{(e)}$	element load vector
Q	the flow rate or discharge per unit width (m$^3\cdot$s$^{-1}\cdot$m^{-1})
y	the free surface elevation measured from an arbitrary datum (m)
Δy^*	correction in y-direction (m)
$\alpha_1, \alpha_2, \alpha_3$	slopes of the velocities at three successive free surface nodes
β	correction factor for the free surface
ε	prescribed accuracy
Γ	boundary of an element
φ	interpolation function
ψ	the stream function (m$^3\cdot$s$^{-1}\cdot$m^{-1})